JMEPEG (2008) 17:202–209
DOI: 10.1007/s11665-007-9136-x

1059-9495/$19.00

Inverse Analysis of Cavitation Impact Phenomena on Structures

S.G. Lambrakos and N.E. Tran

(Submitted April 6, 2007; in revised form May 11, 2007)

A general methodology is presented for in situ detection of cavitation impact phenomena on structures based on inverse analysis of luminescent emissions resulting from the collapsing of bubbles onto surfaces. Following an inverse-analysis approach, luminescent emission signatures are correlated with the general structure of asymmetric bubble collapse onto a surface. This method suggests applications for detection of cavitation that can occur within different types of dynamic water environments of structures. Case study analyses using experimental data are used to demonstrate the fundamentals of various aspects of this methodology. The goal of this methodology is to establish a direct correlation of luminescent emissions with cavitation impact phenomena, and ultimately, with cavitation erosion of structures within turbulent water environments.

Keywords environment, failure analysis, modeling processes, nondestructive testing, surface engineering

1. Introduction

The use of distributed sensors and associated methodologies for the detection of changes in the physical characteristics of processes and in general systems is being developed for a wide range of applications including corrosion monitoring, analysis of surface interactions between chemical and biological species, monitoring of materials deterioration correlated with either damage or failure of a system or structure, and heat transfer within complex structures and processes. System analysis based on distributed sensing is well suited for methodologies based on data-driven inverse analysis, which require the distributed sampling of system responses over relatively large sets of both spatial locations of sensors and changes in physical characteristics of the system.

Sensors are generally categorized according to the method of detection used to correlate changes in the detected signal to changes in a given physical characteristic of the system to be analyzed. This correlation is through a parametric representation of the system that establishes a relationship between input and output quantities. This parametric relationship is based either on a direct- or inverse-problem approach for analysis of systems. This study examines a general method for in situ detection of cavitation impact phenomena within dynamic water environments of structures that is based on inverse analysis of luminescent emissions resulting from cavitation collapse of bubbles onto surfaces. Following an inverse-analysis approach, the shapes of luminescent emission signatures are correlated with the general structure of asymmetric bubble collapse onto a surface. This method suggests applications for detection of cavitation that can occur within different types of dynamic water environments of structures and the assessment of potential cavitation erosion of structures. The method presented here is a generalization of the simplest form of intensiometric sensor, where potential damage is correlated directly with the presence of emission signatures. In that this method is based on inverse analysis, there is no need for a detailed physical representation of the sensor. That is, analysis is accomplished based on the general nature of a given class of data sets and a minimal inverse model parameterization of only the essential response characteristics of the system.

The general approach considered in this study has been applied within the context of several different applications (Ref 1-3). In each case a minimal inverse model parameterization of only the essential response characteristics of the system were employed. In one case an examination was presented of heat transfer, correlated with failure, within a composite fiber cable structure (Ref 1). The essential response characteristic of this type of system for prediction of failure was shown to be that of anisotropic heat transfer. Other physical characteristics of this type of system, such as the geometric configuration of its cross section, and the microscopic and macroscopic structure of the composite fiber system were found to be not relevant for the prediction of failure. In another case an examination was presented of surface degradation, correlated with failure, within corrosive environments (Ref 2). The essential response characteristics of this type of system were those of characteristic average time periods for dissolution of specified thicknesses of a given material within a given corrosive environment. Other physical characteristics of this type of system, such as surface structure and chemical reaction rates for dissolution at the liquid-solid interface where not relevant for prediction of failure. And in still another case an examination was presented of changes in the mechanical performance of a lapjoint structure (Ref 3). The essential characteristics of this system were changes in the response signatures of mechanical

S.G. Lambrakos, Materials Science and Technology Division, Code 6390, Naval Research Laboratory, Washington, DC 20375-5000; and **N.E. Tran,** Chemistry Division, Naval Research Laboratory, Washington, DC 20375-5000. Contact e-mail: lambrakos@anvil.nrl.navy.mil.

vibrational modes correlated with the degradation level of fasteners. For each of the applications considered in Ref 1-3, a prototype system was constructed for the purpose of examining the response characteristics of an individual sensor element in order to establish proof of concept for its extension to a system consisting of distributed sensors for the monitoring of system performance and failure, and prediction of system response using data-driven inverse analysis. For the application considered here, a prototype system is also constructed for the purpose of establishing proof of concept based on inverse analysis. Discussions concerning the direct and inverse problem approaches in general are given in Ref 4-9. Before proceeding, however, a review is presented of aspects of the direct and inverse problem approaches that are relevant to the analysis presented here, in particular.

The direct-problem approach to sensing can be defined as an approach in which the characteristics of the detected signal are predicted using either an explicit numerical solution of equations representing the physical system based on theoretical and computational formulations or an explicit physical model based on an analytical representation of the system. The direct-problem approach requires a priori knowledge of the physical characteristics of the sensor and of its coupling to the environment under detection. Further, this approach requires knowledge of response properties of the materials making up the sensor system.

The inverse-problem approach to sensing can be defined as an approach in which the characteristics of the detected signal are predicted using a model representation whose form is relatively convenient for the adjustment of parameters. The adjustment of parameters is according to experimental data concerning a field quantity, e.g., intensity or current, at various locations that are sufficiently distributed either spatially throughout the environment under detection or parametrically relative to the parameter space representing a specific characteristic of the system. The model representations adopted for an inverse-problem approach can be based on parametric formulations that range from those which include detailed descriptions of the underlying physical interactions or couplings to those characterized by multidimensional interpolation functions whose mathematical-function forms are relatively simple. It is noted, therefore, that an inverse-problem approach to sensing can be applied via any conveniently adjustable parametric representation of the field quantity to be detected.

Direct-problem and inverse-problem formulations posses an interrelationship that is important with respect to analysis based on the inverse-problem approach. An aspect of this interrelationship is that all direct-problem based parametric representations may be adopted for inverse analysis, and that in general, direct-problem analyses can be interpreted as inverse-problem analyses. This interrelationship implies that a reasonable starting point for the formulation of an inverse-problem based parametric representation is to adopt a direct-problem based parametric representation as an initial ansatz for further modification (or optimization) according to the characteristics of the experimental data concerning the field quantities of interest.

In what follows formulation of a method for inverse analysis is presented that is based on the general characteristics of all the processes associated with cavitation bubble collapse onto a surface. Relative to systems identification theory, all processes concerning bubble collapse represent systems whose parameter identification is that of an impulse response. Case study analyses using experimental data are used to demonstrate the fundamentals of various aspects of this method. The results include inverse analysis of measurements of UV and soft x-ray emissions resulting from the cavitation collapse onto surfaces of bubbles in water at ambient pressure. Bubbles were observed to emit photons of energies exceeding 6 eV (wavelengths shorter than 200 nm) as they underwent asymmetric collapse at the surface of a silicon photodiode detector. Each photoemission event consisted of 10^6-10^7 photons with irradiance intensities in excess of 1.4×10^{-6} W/cm^2. Our inverse analysis examines issues concerning the quantitative extraction of features associated luminescent emission signatures as detected and their correlation with cavitation impact phenomena on structures within dynamic water environments.

2. Inverse Analysis of Cavitation Impact Phenomena on Structures

There exist an extensive body of work examining the physical properties of cavitation bubble collapse (Ref 10). In this section, a review is given of certain aspects of these properties that are relevant to the analysis. Depending on boundary and symmetry conditions imposed by an ambient water environment, bubbles can either dissolve or grow until they collapse or fragment into smaller bubbles. With the absence of any solid surface within its near neighborhood, the general morphology of bubble collapse is that shown schematically in Fig. 1a. In the presence of a solid surface, however, the

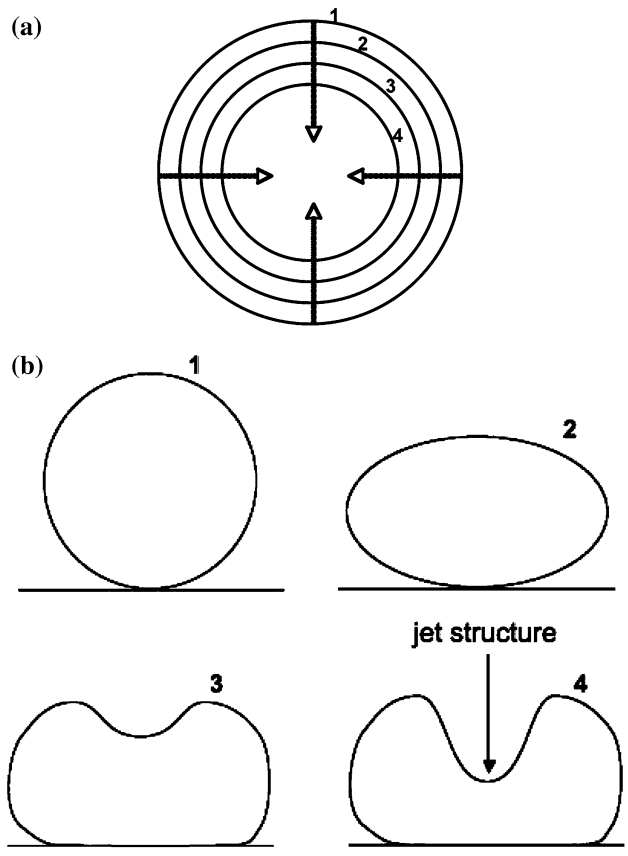

Fig. 1 (a) Schematic representation of cavitation bubble collapse with no solid surface within its near neighborhood, where number sequence denotes progression in time. (b) Schematic representation of cavitation bubble collapse on a solid surface, where number sequence denotes progression in time

general morphology of bubble collapse is that shown in Fig. 1b. Associated with the asymmetric cavitation collapse of bubbles onto surfaces are jet structures (see Fig. 1b), whose morphology is highly correlated with the impulse pressure trace that is observed during collapse of bubbles (see chapter 3 of Ref 10) and ultimately erosion that is due to cavitation.

When subjected to an intense field of ultrasound, bubbles can sustain high-amplitude nonlinear oscillations characterized by cyclic collapse from a maximum radius of approximately 50 μm to that of 0.5 μm, at supersonic speeds approaching 950 m/s (Ref 11-14). The strong periodic compression of the bubble, associated with its cavitation collapse during each cycle, leads to the synchronous induction and emission of localized shock waves (Ref 11, 14, 15) and photons (Ref 16, 17), respectively. The processes of shock induction and photon emission are strongly coupled during the last stages of the cavitation bubble collapse. The complete photoemission spectrum associated with cavitation bubble collapse in water has yet to be determined. Previous studies showed only broad emission bands in the visible region of the electromagnetic wave spectrum characterized by the absence of any spectral peaks (Ref 17-21). The intensity of these spectra appears to increase continuously with frequency until the UV cutoff of water at 200 nm (Ref 18, 21). It is significant to note that there has been no previous evidence of UV emission from the bubble cavitational collapse due to the fact that photons of energies greater than 6 eV tend to be absorbed by water molecules (11, 19). Next, when bubbles sustaining cyclic cavitation collapse due to an ultrasonic field are placed within the near neighborhood of a solid surface, symmetry conditions are disrupted such that the general morphology of cavitation bubble collapse transitions from that of spherically symmetric collapse (Fig. 1a) to that of asymmetric collapse onto a surface (Fig 1b).

At this stage of the presentation it is important to discuss two interrelated issues that are extremely relevant to the proper interpretation of the results of the analysis. One of these issues concerns the nomenclature that is adopted for an accurate description of cavitation processes inducing photoemission measured in this study. The other issue concerns the classification of two distinctly different cavitation processes occurring in the prototype analysis that follows. Ref 22 and references therein have stressed the imprecise nature of the nomenclature "sonoluminescence" owing to the fact that this term has resulted colloquially from the fact that fields of ultrasound, under symmetry conditions, have been typically used in experiments to generate bubbles that grow and collapse cyclically while inducing photoemission. Accordingly, they have suggested that a more precise terminology is that of cavitation luminescence, which represents photoemission resulting from cavitation phenomena in general. This is especially the case for cavitation under asymmetric conditions such as bubble collapse onto surfaces. In the experiments described in the next section two different processes responsible for the induction of cavitation luminescence are to be identified. Only one of these processes, however, is the subject of measurement for our prototype analysis. This process is that of photoemission associated with the asymmetric collapse of a bubble onto a solid surface. The other process, due to an ultrasonic field applied under symmetry conditions, serves only the purpose of isolating a stable bubble at a fixed location in space. Accordingly, any photoemission associated with the dynamic equilibrium of the stable bubble, undergoing periodic growth and collapse, is not relevant to the analysis that follows.

3. Prototype Analysis and Proof of Concept

Presented in this section are fundamentals of a prototype sensor system, and a series of prototype analyses, which have been constructed for the purpose of demonstrating the general inverse-analysis methodology for detection of cavitation using measurements of luminescent emissions.

In this study, an experimental configuration was adopted so that an individual stable bubble (Ref 17) could be generated in an acousto-optic (AO) cell (see Fig. 2) and then made to collapse onto the surface of UV photodiode detectors (International Radiation Detector Inc.). Each photodiode detector adopted for measurement contained a different bandpass filter. One of the photodiodes used for measurement (AXUV100Al) included a directly deposited bandpass filter consisting of an effective silicon filter thickness of 150 nm and bandpass of 17-80 nm, extending into the soft x-ray region of the spectrum corresponding to wavelengths of 1-40 nm (see Fig. 3a). The quantity QE, or quantum efficiency, is defined as the number of electrons detected by an external circuit per incident photon at 100% carrier collection efficiency. The QE of the AXUV100Al photodetector reaches 100% at 2.5 nm and 347% at 0.94 nm (see inset of Fig. 3a). The other photodiode used for measurements (AXUV100LA) included a directly deposited bandpass filter consisting of an effective silicon filter thickness of 200 nm and bandpass of 117-131 nm (see Fig. 3b). The highest

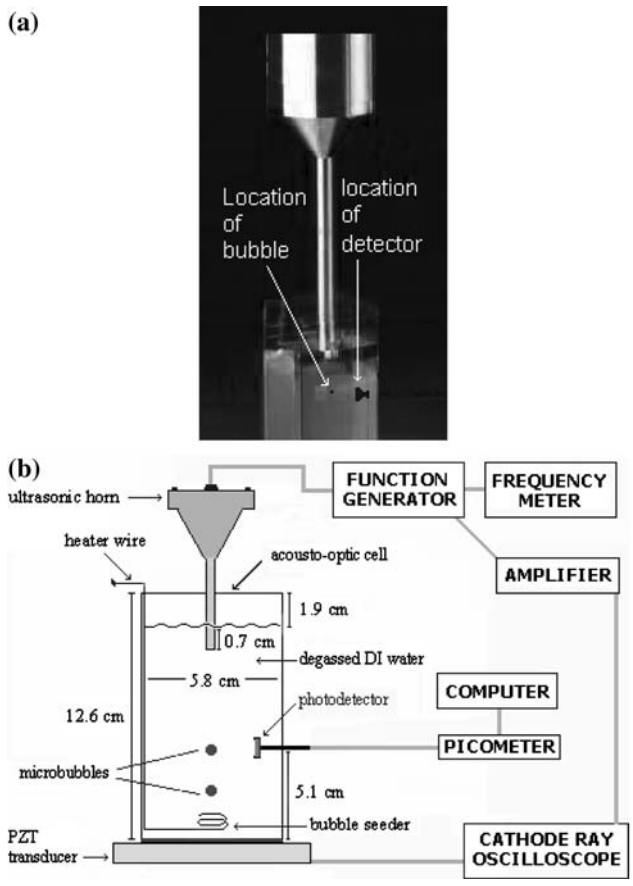

Fig. 2 (a) Experimental configuration for generation of an individual stable bubble using an acousto-optic (AO) cell. (b) Schematic representation of experimental arrangement of AO-cell used for the generation of a single hydrated bubble

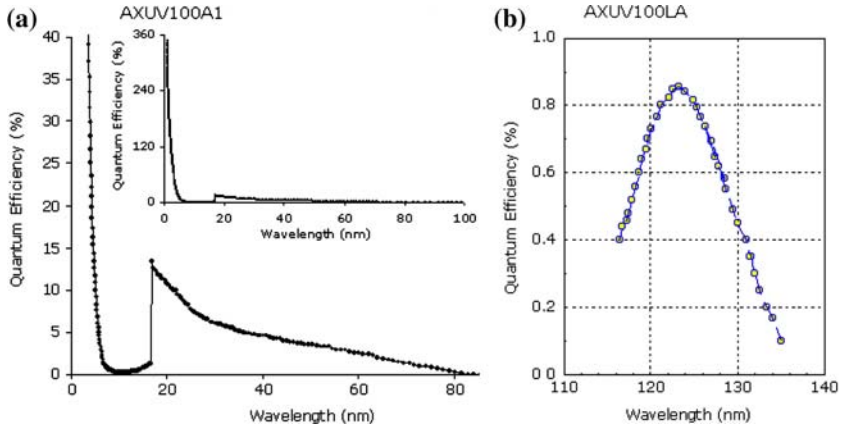

Fig. 3 Quantum efficiency (QE) as a function of wavelength for models AXUV100A1 (a) and AXUV100LA (b) silicon photodetectors. The inset in (a) shows the quantum efficiency of the 0.94-100 nm-range bandpass filter. Data were provided by the International Radiation Detectors, Inc.

quantum efficiency (QE_{max}) of the AXUV100LA photodetector is 85%, which occurs at 124 nm. The incident photon energy, E_{ph}, can be estimated using the relation $E_{ph} = 3.7 \times QE$ (eV), based on the reference provided by IRD Inc. The flux of incident photons (photons/cm^2 s) that are incident onto the photodiode detector detected by the DC external circuit can be estimated as follows:

$$N = \frac{I \cdot s}{A \cdot r \cdot \bar{E} \cdot e} \quad \text{(Eq 1)}$$

where I is the average current produced in the photodiode, s is the ionization constant in silicon (3.63 eV/electron-hole pair (Ref 23, 24), A is the area of the diode (1.0 cm^2 for both AXUV100LA and AXUV100Al), r is the diode detection efficiency (assumed a constant of 0.01), $\bar{E}$ is the average energy of Compton-recoil electrons in the detector (expressed in eV), and e is the electron charge (1.602×10^{-19} coulombs). The quantity $\bar{E}$ can be estimated as 1/2 $\bar{E}_{max}$, where $\bar{E}_{max}$ is derived from Compton's formula for the energy of a backscattered photon (i.e., a photon whose scattering angle is 180°) (Ref 24). The quantity $\bar{E}_{max}$ is given by:

$$\bar{E}_{max} = hv\left[\frac{2hv}{m_o c^2 + 2hv}\right] \quad \text{(Eq 2)}$$

where hv is the energy of the incident photon ($h = 4.135 \times 10^{-15}$ eV s), c is the speed of light (2.9979×10^{10} cm/s), and the values of $m_o c^2$ for the model AXUV100A1 and AXUV100LA silicon photodetectors are 523.82 and 65.83 eV, respectively.

Deionized (DI) water (resistivity = 18.2 M ω cm, pH = 5.3, T = 25 °C) was degassed under vacuum in a hot water bath for 10 min and then in an ice bath for 1 h until the temperature of the DI water reached about 4 °C (pH = 6.1). At the temperature of 4 °C, water achieves its highest density, 1.000 g/L, and accordingly, the photoemission occurring during the collapse of a hydrated bubble is expected to be the brightest, which is consistent with the experimental observations in this study. Approximately 306.0 mL of the DI water was transferred to the AO-cell at an angle at a relatively slow flow rate in order to avoid regassing the water. The transmitting element of an ultrasonic horn (Sonoluminescence.com, Fig. 2) was positioned at the center of the AO-cell such that the tip of the horn transmitter was submerged approximately 0.7 cm below the surface of the water. The resonance frequency of the AO-cell was located using an oscilloscope (Tecktonix, TAS 465) in conjunction with a function generator (Ramsey SG-550 Audiogenerator from Sonoluminescence.com). The resonance frequency was varied between 26.4 and 27.6 kHz, and was dependent on the temperature of the DI water. The higher the temperature of the water, the higher the driving resonance frequency required for stabilizing the bubble. The nucleation of the bubble was initiated via a transient current through the heater wire. Once a stable bubble emitting blue light was observed, the UV filter diode detector was immediately directed toward the bubble and induced the bubble collapse on the photodetector surface. The UV emissions resulting from the collapse of the bubble onto the solid plane surface of the photodetector were then recorded by a picometer (Keithley 6485).

Shown in Fig. 2b is a schematic representation of experimental arrangement of AO-cell used for the generation of a single hydrated bubble. The vertical acoustic wave field is maintained within the volume of water by two parallel piezoelectric transducers (PZTs) located at the top (inside the acoustic horn, not shown) and bottom of the cell. The bubble seeder is a coiled nichrome wire (0.5 mm diameter) attached to an electric boiler. The position of the UV detector is adjusted during the experiment in order to detect the ultrashort (~1 ns) photoemissions originating from the top bubble, which was typically observed to be the brightest. The function generator was set between 26.4 and 27.6 kHz, corresponding to frequencies within the neighborhood of the resonance frequency of the AO-cell. The operating voltage required for sustaining the stability of the top bubble was found to vary between 2.5 and 3.5 V.

It was observed during the experiment that moving the detector toward the blue-glowing bubble slowly tended to cause the bubble to move away from the detector and eventually extinguish because of the breakdown of symmetry conditions for standing wave excitation. When the detector was moved quickly toward the bubble, however, the bubble momentarily adhered to the solid plane of the detector before it collapsed. In this later case, the timescale of the spectral signal collected varied between 60 ms (equivalent to 1500 cyclic cavitations or

Table 1 Summary of calculations based on UV emissions spectra shown in Fig 3

Photodiode	λ, nm	I_{ave}, A	hv, eV	$\bar{E}$, eV	N, photons/cm^2 s	Photon, s/flash	W/cm^2
AXUV100LA	117-131	3.8×10^{-10}	0.41	0.14	4.09×10^{12}	3.14×10^{8}	1.38×10^{-7}
AXUV100A1	17-80	1.4×10^{-8}	23.29	7.76	6.28×10^{12}	2.04×10^{8}	5.08×10^{-6}

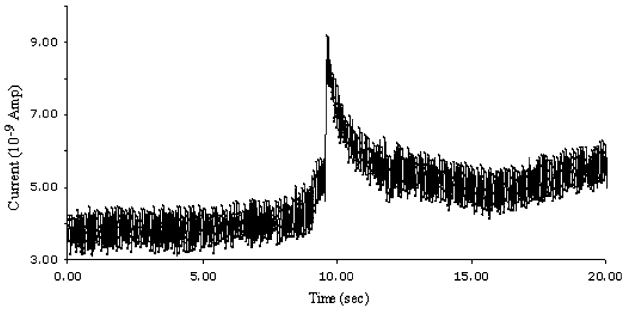

Fig. 4 Photo-current as a function of integrated response time of the AXUV100LA photodetector with a 117-131 nm bandpass showing impulse response signature

photoemission events of the bubbles, inset of Fig. 3a) and 800 ms (equivalent to 20,000 cyclic cavitations, Fig. 3b); the duration of each acoustic cycle is about 40 μs at 4 °C for the AO-cell. The average currents collected from the bandpass filters of AXUV100A1 (wavelengths λ = 17-80 nm) and AXUV100LA silicon photodetector (wavelengths λ = 117-131 nm) are 1.4×10^{-8} and 3.8×10^{-10} A, respectively. The irradiance intensity (I_o) of the bubble photoemission detected by AXUV100A1 and AXUV100LA detectors are 5.08×10^{-6} and 1.38×10^{-6} W/cm^2, respectively. Other relevant data concerning these detectors are given in Table 1.

The impulsive signature response of the detected signal (see Fig. 4) appears to have the general morphology of cavitation bubble collapse at a solid surface. The rapid increase in current across the discontinuity observed in Fig. 4 is a well-known characteristic of shockwave signature structure (Ref 25). It follows that the photoemission originates from the collapsing surface and is strongly correlated with the speed of the asymmetrically collapsing surface. Accordingly, the inverse analysis of cavitation impact phenomena adopts as its model representation that of a collapsing liquid-vapor interface (Fig. 1b) that imparts an impulsive load to a surface while coincidentally emitting photons. Again, the concern is not the mechanism for origination of these photons, but rather that one is able to assume with reasonable certainty a direct correlation between a photon emission signature as detected and the occurrence of localized impulsive loading on a solid surface due to cavitation bubble collapse.

4. Signature Analysis

As indicated above, the methodology presented here is based on the simplest form of intensiometric sensor, where damage or failure is correlated with a convenient measure of relative change in signal, avoiding the need for a detailed physical representation of the sensor. In that this method adopts an essentially yes/no criterion for detection, as in the analyses presented in references (Ref 1-3), parameter sensitivity is determined according to changes in detected signal that are relative to a zero signal, rather than according to a specified fractional change in signal. Accordingly, any error analysis or filtering of signals must be applied according to this criterion for signal detection. For the present analysis, the structure of the signal to be detected is that of a singular spike, which is characteristic of an impulsive response of a system.

Table 2 Bubble collapse events observed for each series of emission signal measurements

UV	BCE	UV	BCE	UV	BCE
1	1	4	2	7	51
2	1	5	7	8	38
3	1	6	26	9	40

Shown in Figs. 5 and 6 are photoemission spectra taken by photodiode detectors in UV and soft x-ray regions, respectively. We consider first spectra and associated signature structure of the detected signals for UV emissions (Fig. 5). Referring to Fig. 5, one can observe impulse signatures that are characteristic of bubble collapse onto a solid surface. During the measurement of these signals a visual count was made of the number of bubble collapse events (BCE) in order to establish confirmation of correspondence between bubble collapse events and measured impulse signatures. Accordingly, for the detected signals shown in Fig. 5, the corresponding numbers of observed bubble collapse events are given in Table 2.

Next, consideration is given of spectra and associated signature structure of the detected signals for soft x-ray emissions (Fig. 6). Referring to Fig. 6, although signal-to-noise characteristics of the detector do not permit resolution of any high-order signature structure, one can observe impulse signatures that are characteristic of bubble collapse onto a solid surface. During the measurement of these signals a single bubble collapse event was observed visually.

The conceptual foundation of the methodology follows from the fact that each of the singular spikes, or characteristic impulse response signatures, shown in Figs. 5 and 6 is associated with an observed bubble collapse event. It is significant to note that this correlation is independent of any background spectral structure that may be associated with the cavitation luminescence process as well as the nature of its detection. A review of the various trends for the measured signals of photoemission shown in Fig. 5, indicates that these spectra contain additional information concerning cavitation luminescence and its detection, which is related to bubble collapse morphology in the neighborhood of a solid surface and to characteristic timescales for photo-detection of cavitation luminescence. Referring to Fig. 5, it is to be noted that in particular all characteristic impulse response signatures are essentially uncoupled from background spectral structure. This uncoupled nature of the impulse response signatures is a fundamental aspect of the inverse-analysis approach considered

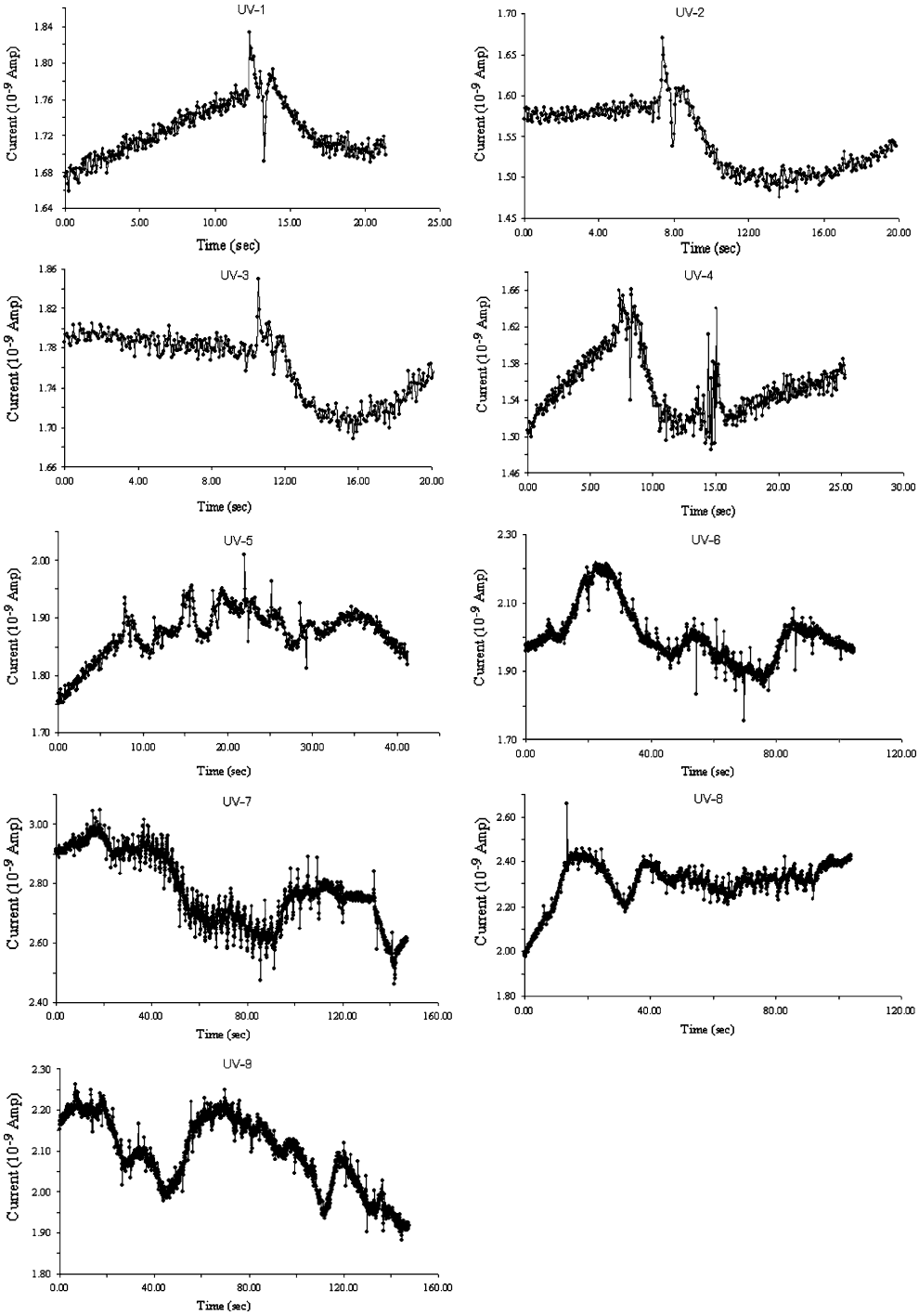

Fig. 5 Photo-current as a function of integrated response time of the AXUV100LA photodetector with a 117-131 nm bandpass corresponding to different numbers of sequential bubble collapse events

here, which eliminates the requirement of considering many of the complex factors associated with cavitation bubble collapse and its detection.

5. Discussion

At this point a review is given of elements of the general sensor methodology with reference to the prototype analysis described above.

1. There exist readily available detector technology, e.g., AXUV100A1 and AXUV100LA silicon photodetectors described above, for detection of photo emission correlated with cavitation impact phenomena. As demonstrated, detection of photoemission can span a relatively wide range of emission frequencies, e.g., UV to soft x-ray.
2. The general characteristics of the measured emissions suggest that analysis in terms of detailed relationships between bubble morphology associated with cavitation

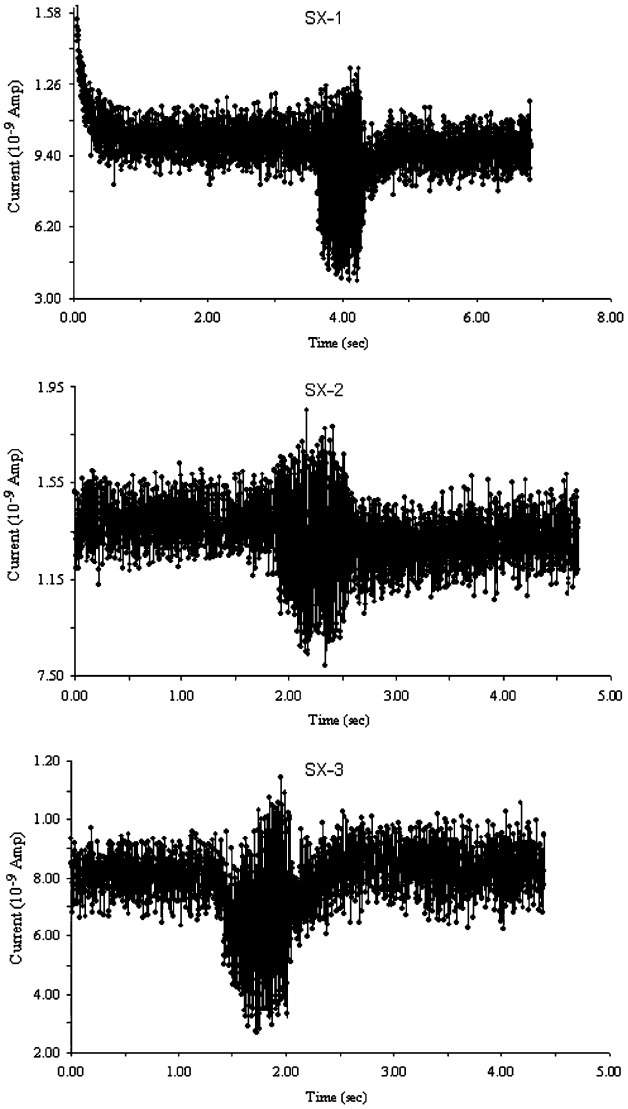

Fig. 6 Photo-current as a function of integrated response time of the AXUV100A1 photodetector with a 17-80 nm bandpass corresponding to a single bubble collapse event

impact and emission signatures, i.e., the direct-problem approach, may not be well posed for certain applications, or in general, extremely difficult. This follows from the typically observed signal-to-noise ratios for the specific sensor methodology considered here and in the work of others who have investigated cavitation luminescence using a direct-problem approach (see Ref 22 and references therein).

3. An inverse-analysis approach employing a minimal parametric representation of the structure of emission signatures should be well posed for correlating detected signals with cavitation bubble collapse events on surfaces. This follows from the above analysis, which indicates that an impulse response signature, i.e., a singular spike, can be directly correlated with cavitation bubble collapse onto surfaces. This simple structure is sufficient for determining the presence of cavitation impact phenomena that could potentially lead to cavitation erosion of structures.

Although the prototype analysis presented here is sufficient for demonstrating that a general methodology can be based on correlating impulse response signatures with cavitation bubble collapse on surfaces, the optimum implementation of a sensor system based on this methodology, as well as the associated post processing or filtering of detected signals, remains an open question. For example, a potential issue may be related to the detection of multiple sequential collapse of bubbles in contrast to the detection of relatively isolated bubble collapse events, e.g., UV-7 in contrast to UV-1 in Fig. 5. It is significant to note, however, that impulse response signatures (or singular spikes) directly correlated with bubble collapse events are observable in both cases, and therefore does not represent a problem in principle. Another potential issue may concern water preparation, i.e., degassing and cooling, with respect to convenience for analysis of cavitation impact phenomena for a given system.

6. Conclusion

The results of the analysis presented here support the feasibility of the development of methodologies for inverse analysis of cavitation impact phenomena on structures. These also indicate, however, significant issues associated with the detection of cavitation emission signatures related to signal-to-noise ratios and detection frequency. These results are consistent with those of previous studies, whose goal was the detection of photoemissions for practical application related to cavitation degradation of structures (Ref 22 and references therein). The analysis of the photoemissions of bubbles in the UV and soft x-ray regions provides new information related to the transduction of bubble cavitation into high-energy photons. It is significant to note that this phenomenon still remains a puzzle today, as when it was first reported by Frenzel and Schultes (Ref 16). The primary interest in the present study, however, is not the mechanism for transduction of cavitation into photons (the direct-problem approach), but rather that this photon emission can be directly correlated with the presence of cavitation impact phenomena. Accordingly, the conceptual foundation of the analysis approach presented here is that of correlating relatively qualitative first-order characteristics of the response signature structure to cavitation impact phenomena. Reference to Figs. 5 and 6, however, indicates that the measured emission spectra contain additional information related to cavitation bubble collapse phenomena in terms of both signature structure and time series characteristics.

Acknowledgments

This research was supported by a Naval Research Laboratory core program related to data-driven inverse analysis of materials and system response and the Office of Naval Research. The authors would like to thank Dr Valerie Browning for her discussions concerning cavitation collapse of bubbles.

References

1. P.G. Moore, H.N. Jones III, and S.G. Lambrakos, An Inverse Heat Transfer Model of Thermal Degradation Within Multifunctional Tensioned Cable Structures, *J. Mater. Eng. Perform.*, 2005, **14**(1), p 112–118

2. S.G. Lambrakos, N.E. Tran, N. Lagakos, and P.P. Trzaskoma-Paulette, Inverse Analysis of Surface Degradation using Optical Fibers, *J. Mater. Eng. Perform.*, 2006, **15**(4), p 484–489
3. H.N. Jones III, N. Lagakos, S.G. Lambrakos and P.P. Trzaskoma-Paulette, Assessment of Mechanical Strength Degradation Using an Embedded Fiber Optic Sensor, *J. Mater. Eng. Perform*., DOI: 10.1007/s11665-007-9130-3
4. K.A. Woodbury eds., *Inverse Engineering Handbook*. CRC Press, New York, 2003
5. A. Tarantola, *Inverse Problem Theory and Methods for Model Parameter Estimation*. SIAM, Philadelphia, PA, 2005
6. C.R. Vogel, *Computational Methods for Inverse Problems*. SIAM, Philadelphia, PA, 2002
7. P.C. Sabatier eds., *Inverse Problems: An Interdisciplinary Study.* Academic Press, London, 1987
8. C.W. Groetsch, *Inverse Problems in the Mathematical Sciences*. Vieweg, Bruanschweig, Wiesbaden, 1993
9. A. Kirsch, *An Introduction to the Mathematical Theory of Inverse Problems*. Springer Verlag, New York, 1996
10. C.E. Brennen, *Cavitation and Bubble Dynamics*, 1995, Oxford University Press
11. M.P. Brenner, S. Hilgenfeldt, and D. Lohse, Single-bubble sonoluminescence, *Rev. Mod. Phys.*, 2002, **74**, p 425
12. B.P. Barber, R. Hiller, K. Arisaka, H. Fetterman, and S. Putterman, Resolving the Picosecond Characteristics Of Synchronous Sonoluminescence, *J. Acoust. Soc. Am.*, 1992, **91**(5), p 3061–3063
13. B. Gompf and R. Pecha, Mie Scattering from a Sonoluminescing Bubble with High Spatial and Temporal Resolution, *Phys. Rev. E*, 2000, **61**, p 5253
14. W.C. Moss, D.B. Clarke, J.W. White, and D.A. Young, Hydrodynamic Simulations of Bubble Collapse and Picosecond Sonoluminescence, *Phys. Fluids*, 1994, **6**, p 2979–2985
15. K.R. Weninger, P.G. Evans, and S.J. Putterman, Time Correlated Single Photon Mie Scattering from a Sonoluminescing Bubble, *Phys. Rev. E*, 2000, **61**, p R1020
16. H. Frenzel and H. Schultes, Lumineszenz im ultraschallbeschickten Wasser, *Z. Phys. Chem. Abt B*, 1934, **27**, p 421–424
17. D.F. Gaitan, L.A. Crum, C.C. Church, and R.A. Roy, Sonoluminescence and Bubble Dynamics for a Single Stable Cavitation Bubble, *J. Acoust. Soc. Am.*, 1992, **91**, p 3166–3183
18. R. Hiller, S.J. Putterman, and B.P. Barber, Spectrum of Synchronous Picosecond Sonoluminescence, *Phys. Rev. Lett.*, 1992, **69**, p 1182–1184
19. T.J. Matula, R.A. Roy, P.D. Mourad, W.B. McNamara, and K.S. Suslick, Comparison of Multibubble and Single-Bubble Sonoluminescence Spectra, *Phys. Rev. Lett.*, 1995, **75**, p 2602–2605
20. R. Hiller and S.J. Putterman, Observation of Isotope Effects in Sonoluminescence, *Phys. Rev. Lett.*, 1995, **75**, p 3549
21. B.P. Barber, R.A. Hiller, R. Lofstedt, S.J. Putterman, and K.R. Weninger, Defining the Unknowns of Sonoluminescence, *Phys. Rep.*, 1997, **281**, p 65–143
22. T.G. Leighton, M. Farhat, J.E. Field, and F. Avellan, Cavitation Luminescence from Flow over a Hydrofoil in a Cavitation Tunnel, *J. Fluid. Mech.*, 2003, **480**, p 43–60
23. K.F. Glenn, *Radiation Detection and Measurement*. John Wiley and Sons, New York, 1979, 25–33
24. D.S. Gray, S.C. Luckhardt, L. Chousal, G. Gunner, A.G. Kellman, and D.G. Whyte, Time Resolved Radiated Power during Tokamak Disruptions and Spectral Averaging of AXUV Photodiode Response in DIII-D, *Rev. Sci. Instrum.*, 2004, **75**, p 376
25. V.L. Jacobs, "Radiation-Hydrodynamics Approaches to Laser-Matter Interactions and Shock-Wave Phenomena," Naval Research Laboratory, NRL/MR/6690—94-7621, 1994, p 107–120